

Dynamics of dissipative multiple exciton generation in nanocrystals

Maryam Azizi and Paweł Machnikowski

Institute of Physics, Wrocław University of Technology, 50-370 Wrocław, Poland

(Dated: May 2, 2022)

The population dynamics of single- and bi-exciton states in semiconductor nanocrystals is modeled numerically in the presence of Coulomb coupling between single- and two-exciton states and a dissipation channel in order to study the transient bi-exciton population that occurs in an optically excited semiconductor nanocrystal. The results show that the system evolution strongly changes if the dissipation is included. In a certain range of parameters, the growth of the exciton number (MEG process) is fast (on picosecond time scale) and the following decay (Auger process) is much slower (hundreds of picoseconds). In some cases, the maximum occupation of the bi-exciton state increases when dissipation is included. The dynamics of an ensemble of nanocrystals with a certain size dispersion is studied by averaging over the energy of the bi-exciton state which can be different for each single nanocrystal. The validity of Markov and secular approximation is also verified.

I. INTRODUCTION

One of the possible ways of improving the efficiency of the existing solar cells is to exploit the process of multiple exciton generation (MEG) in semiconductor nanocrystals (NCs)¹. Such an effect consists in generation of two or more electron-hole pairs by a single high energy photon and thus converts the excess above-bandgap energy into useful current. This process is enabled by Coulomb coupling between single-pair (exciton, X) states and two-pair (biexciton, BX) states in a NC (or, in general, between states with n and $n + 1$ pairs) and consists in an intraband relaxation of a carrier (typically an electron, due to larger energy scales of confined states in the conduction band) accompanied by a creation of a new electron-hole pair (an inverse Auger process). In this way, the excess energy obtained by an electron upon absorbing a high-energy photon is not dissipated in a phonon relaxation processes and becomes available for photovoltaic conversion.

The initial experimental results, showing very high values of the quantum efficiency of photoconversion in various systems^{2–9}, were subsequently reinterpreted^{10–14} based on the growing understanding of the experimental difficulties that might lead to overestimating the achieved numbers of excitons per single absorbed photon^{15–17}. Nonetheless, more recent experiments on real NC-based solar cell devices^{18,19} do provide a direct proof of the usefulness of this process in solar energy conversion. Theoretically, the description of the X and BX spectrum and the X-BX couplings that are essential for the MEG process has been proposed using the methods of density functional^{20,21}, pseudopotential^{22–25}, tight binding^{26–29}, and $k \cdot p$ theory^{30–32}.

Along with the investigation of these structural properties, much attention has been devoted to the carrier dynamics in a nanocrystal under optical excitation at energies high enough to generate multiple excitons, in particular to the role of decoherence and relaxation. These studies included dynamical simulations of few-level models^{30,33} as well as of many-level models aiming at re-

producing the density of X and BX states in the high-energy sector of a nanocrystal^{29,31,34–36}. In many cases, dissipative effects are included in these models on a phenomenological level and expressed by a number (usually small) of dephasing rates^{26,30,31,33}. In this way, the multiple exciton generation could be described as a process competing with exciton relaxation^{30,31} and, in certain cases, suppressed by coupling to the dissipative environment (typically considered to be phonons)²⁶.

In this paper, we study the time evolution of the X-BX system within a minimal, three-level model that accounts both for the impact ionization and Auger recombination in the presence of dissipation. Expressing the couplings to the environment in a generic form in terms of a physically motivated set of spectral densities allows us to characterize the emerging coupling to the Coulomb-correlated X-BX eigenstates and to discuss the dependence of the rates of various phonon-assisted processes (relaxation and impact ionization) on the Coulomb coupling itself. We show that, on the general level, the dissipative MEG process is determined by the same couplings to the dissipative environment as the carrier relaxation and dephasing. Furthermore, we find out that the system dynamics realizes various dynamical scenarios, depending on the alignment of the X and BX levels and on the relation between the level spacing and the spectral properties of the coupling to the environment (in particular, the high-frequency cut-off of the spectral density). As we show, the presence of dissipation considerably modifies the system dynamics and, in many cases, increases the efficiency of the MEG process. We study also the role of the excitation conditions (pulsed, continuous wave or incoherent thermal) and show that the strong differences between the system kinetics under different excitation conditions³³ are washed out by dissipation. Finally, we assess the validity of Markov and secular approximations for the description of dissipation-assisted MEG in nanocrystals.

The paper is organized as follows. In Sec. II, we define the model (Sec. II A), describe the Master equations for the system evolution (Sec. II B), and discuss the for-

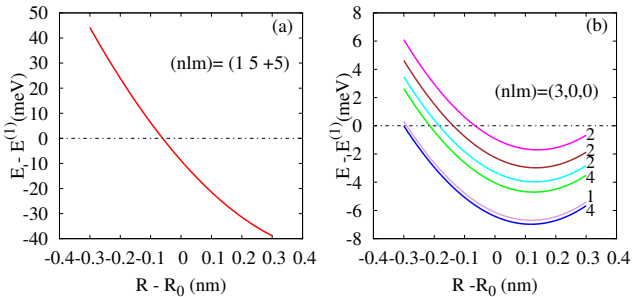


FIG. 1. (Color online) Relative energy of BX states in vicinity of selected bright X states with quantum numbers as indicated as a function of the NC radius around $R_0 = 3$ nm. The numbers on the right denote degeneracy.

mal structure of the carrier-environment coupling in a NC (Sec. II C). In Sec. III, the results of our simulations are discussed: first the dynamics in the Markov limit is studied (Sec. III A) and then non-Markovian corrections are discussed (Sec. III B). Finally, Sec. IV concludes the paper.

II. MODEL

A. The system

Although the density of BX states in a nanocrystal is very high, only a few tens of them are coupled to a given bright X state³⁷. Moreover, usually only a few coupled BX states lie in the vicinity of the X state while vast majority of them is relatively distant. In Fig. 1, we show two selected examples of the spectral positions of BX states relative to selected X states to which they are coupled (the quantum numbers for the selected exciton states are the same for the electron and the hole and are shown in the figure). This approximate result is obtained within the single-band envelope function approximation with Coulomb interactions included in the lowest order for an InAs nanocrystal with the radius R close to $R_0 = 3$ nm^{37,38}. As can be seen, only one or a few BX states appear in the spectral vicinity of a given X state. Thus, the essential features of the MEG dynamics can be expected to be determined by impact ionization within groups of a few states.

Consider an optically active (bright) excited X state of a NC. At lower energies, other X states are present to which the carriers can relax. For our purpose, it is sufficient to consider one such level. We will consider situations in which a BX state Coulomb-coupled to the bright X state is present in between the two X states, which is a common situation for highly excited X states, where the coupled BX states are rather dense. Taking into account the selection rules for interband Coulomb couplings³⁷, it is rather unlikely that this BX state will also be coupled to the other, lower X state. Therefore, for

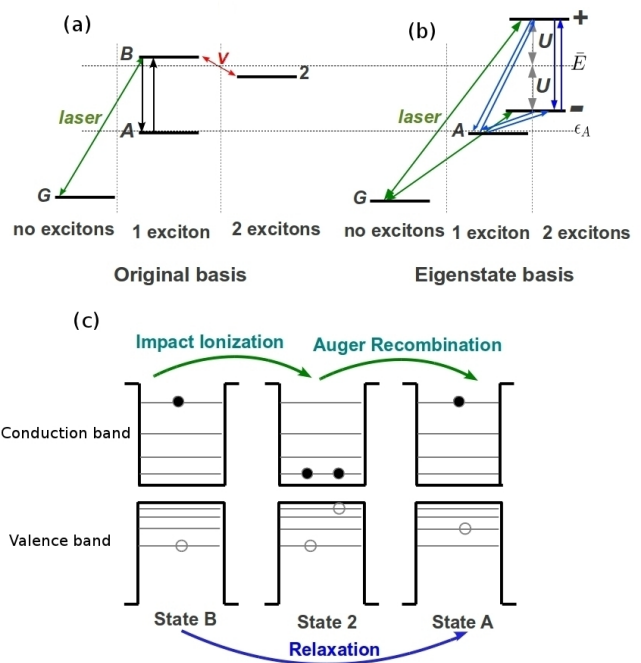


FIG. 2. (Color online) (a) The schematic diagram of system states and couplings. The green arrow shows the laser excitation while the black arrows represent the environment-induced transitions. The Coulomb coupling between X and BX configurations is shown with a red arrow. (b) The diagram of system eigenstates with the optical excitation paths (green) and environment-induced transitions (blue). (c) Graphical representation of the processes involved.

our dynamical modeling, we consider a four-level model of a nanocrystal, as shown in the Fig. 2(a). Here the state G refers to the ground state (empty nanocrystal), A and B denote the two X states and 2 is the BX state. We assume that the BX state 2 is coupled only to the state B by a Coulomb coupling V which is taken to be a real parameter.

The Hamiltonian of the carrier system is then

$$H_0 = \epsilon_A |A\rangle\langle A| + \epsilon_B |B\rangle\langle B| + \epsilon_2 |2\rangle\langle 2| + V(|B\rangle\langle 2| + |2\rangle\langle B|), \quad (1)$$

where ϵ_A, ϵ_B and ϵ_2 are the energies of the states A, B and 2 respectively. We set the energy of the ground state to be zero. Moreover, the system is excited by a classical light pulse which has the frequency Ω close to the $G \longleftrightarrow B$ transition. By standard selection rules, this pulse couples the ground state only to the X states. We assume that only the state B is bright. The corresponding Hamiltonian of the excitation is

$$H_{\text{las}} = \frac{1}{2} f(t) (|G\rangle\langle B| e^{i\Omega t} + |B\rangle\langle G| e^{-i\Omega t}). \quad (2)$$

In addition, the system undergoes dissipative dynamics due to the interaction with its environment. We do not assume any specific form of the coupling to the environment and aim at a model which is independent of the

nature of this coupling. The only restriction on this coupling is that in the absence of Coulomb-induced mixing between the X and BX configurations no interband processes are allowed [see Fig. 2(a)]. Thus, the interaction with the environment can be described by the following Hamiltonian

$$H_{\text{int}} = |A\rangle\langle A|\mathcal{R}_{AA} + |B\rangle\langle B|\mathcal{R}_{BB} + |2\rangle\langle 2|\mathcal{R}_{22} + |A\rangle\langle B|\mathcal{R}_{AB} + |B\rangle\langle A|\mathcal{R}_{BA}, \quad (3)$$

where $\mathcal{R}_{\alpha\beta}$ (with $\alpha, \beta = A, B, 2$) are certain environment operators with the property $\mathcal{R}_{\alpha\beta} = \mathcal{R}_{\beta\alpha}^\dagger$.

The system evolution is described in the basis of eigenstates of H_0 : $|G\rangle$, $|A\rangle$, $|+\rangle$ and $|-\rangle$, where $|+\rangle$ and $|-\rangle$ result from the Coulomb coupling between the X state $|B\rangle$ and the BX state $|2\rangle$,

$$\begin{aligned} |+\rangle &= \cos(\theta/2)|B\rangle + \sin(\theta/2)|2\rangle, \\ |-\rangle &= -\sin(\theta/2)|B\rangle + \cos(\theta/2)|2\rangle, \end{aligned} \quad (4)$$

Here, θ is the mixing angle, defined by $\tan \theta = 2V/(\epsilon_B - \epsilon_2)$, which is close to 0 for weakly mixed X and BX states and goes to $\pm\pi/2$ if a nearly degenerate pair of X and BX states is strongly coupled. The energies of these states are $E_\pm = \bar{E} \pm U$, where $\bar{E} = (\epsilon_B + \epsilon_2)/2$ and $U = [(\epsilon_B - \epsilon_2)^2/4 + V^2]^{1/2}$. In the eigenstate basis, the interaction Hamiltonian can be written as

$$H_{\text{int}} = \sum_{i,j=A,\pm} \sigma_{ij} \tilde{\mathcal{R}}_{ij}, \quad (5)$$

where $\sigma_{ij} = |i\rangle\langle j|$ and

$$\tilde{\mathcal{R}}_{A+} = \cos \frac{\theta}{2} \mathcal{R}_{AB}, \quad \tilde{\mathcal{R}}_{A-} = -\sin \frac{\theta}{2} \mathcal{R}_{AB}, \quad (6a)$$

$$\tilde{\mathcal{R}}_{\pm\pm} = \frac{1}{2} (\mathcal{R}_{BB} + \mathcal{R}_{AA}) \pm \frac{1}{2} \cos \theta (\mathcal{R}_{BB} - \mathcal{R}_{AA}), \quad (6b)$$

$$\tilde{\mathcal{R}}_{+-} = \frac{1}{2} \sin \theta (\mathcal{R}_{22} - \mathcal{R}_{BB}), \quad (6c)$$

with $\tilde{\mathcal{R}}_{ij}^+ = \tilde{\mathcal{R}}_{ji}$.

B. Evolution: Master equation

While Markov approximation has commonly been used to model the dissipation effect on the MEG process in nanocrystals (often on the level of phenomenological dephasing rates)^{29–31,33–36}, its validity is not obvious for the present system. Indeed, as observed in experiment and reproduced by our simulations discussed below, only the Auger recombination phase of the system dynamics is slow, while the initial impact ionization dynamics takes place on much shorter, picosecond time scales. Therefore, in this paper, we will compare the Markovian dynamics with a more general approach, where the reservoir memory is taken into account. In both cases, the evolution of the system will be described in the density matrix

formalism by solving the appropriate quantum Master equation.

Thus, the starting point for our modeling of the system evolution is the time-convolutionless Master equation for the reduced density matrix of the charge subsystem in the NC in the lowest order. In the interaction picture, this equation has the form³⁹

$$\dot{\tilde{\rho}} = -\frac{1}{\hbar^2} \text{Tr}_R \int_0^t d\tau [H_{\text{int}}(\tau), [H_{\text{int}}(\tau), \tilde{\rho}(\tau) \otimes \rho_R]], \quad (7)$$

where $H_{\text{int}}(t)$ and $\tilde{\rho}$ are the interaction Hamiltonian and the reduced density matrix of the nanocrystal in the interaction picture, ρ_R is the density matrix of the reservoir at thermal equilibrium, and Tr_R denotes the partial trace over the reservoir degrees of freedom. Upon substituting the interaction Hamiltonian from Eq. (5) and taking the partial trace this yields

$$\begin{aligned} \dot{\tilde{\rho}}(t) &= -\frac{1}{2} e^{i(\omega_i - \omega_j + \omega_k - \omega_l)t} \\ &\quad \times \Gamma_{ijkl}(t) [\sigma_{ij} \sigma_{kl} \tilde{\rho}(t) - \sigma_{kl} \tilde{\rho}(t) \sigma_{ij}] + \text{h.c.}, \end{aligned} \quad (8)$$

with $\omega_i = E_i/\hbar$ and the time-dependent rates

$$\Gamma_{ijkl}(t) = \frac{2}{\hbar^2} \text{Re} \sum_{ijkl} \int_0^t ds e^{i(\omega_l - \omega_k)s} \langle \tilde{\mathcal{R}}_{ij}(s) \tilde{\mathcal{R}}_{kl} \rangle, \quad (9)$$

where $\tilde{\mathcal{R}}_{ij}(s)$ denotes the operator $\tilde{\mathcal{R}}_{ij}$ in the interaction picture with respect to the reservoir Hamiltonian and we have neglected the imaginary parts of the rates that describe reservoir-induced energy shifts.

The reservoir correlation function (“memory function”) $\langle \tilde{\mathcal{R}}_{ij}(s) \tilde{\mathcal{R}}_{kl} \rangle$ is related to the spectral density

$$\tilde{R}_{ijkl}(\omega) = \frac{1}{2\pi\hbar^2} \int dt e^{i\omega t} \langle \tilde{\mathcal{R}}_{ij}(t) \tilde{\mathcal{R}}_{kl} \rangle, \quad (10)$$

for $i, j, k, l = A, \pm$, which fully characterizes the dissipative coupling to the environment. In the same way, spectral densities $\mathcal{R}_{\alpha\beta\gamma\delta}(\omega)$ are defined in terms of correlation functions between the operators $R_{\alpha\beta}$ in the original basis [Eq. (3)]. If the reservoir correlations decay on a certain time scale (reservoir memory time) then, on longer time scales, the rates become constant and equal to

$$\Gamma_{ijkl}(t) \xrightarrow{t \rightarrow \infty} \Gamma_{ijkl}(\infty) = 2\pi R_{ijkl}(\omega_l - \omega_k).$$

Moreover, as follows from Eq. (9), in the absence of degeneracy, the rates other than Γ_{ijji} and Γ_{iiji} contain an oscillating factor and can be assumed to be small if the separation of the levels is large and the overall system dynamics is slow. Therefore, it is common to use the secular approximation where the terms containing such oscillating rates are neglected. The rates of the type Γ_{iiji} at long times are proportional to the corresponding spectral density at zero frequency, which vanishes in many common situations (super-Ohmic reservoirs and Ohmic reservoirs at zero temperature, see below). Thus, one reaches the commonly used Markov approximation with

the evolution equation in the Lindblad form³⁹, which in the Schrödinger picture can be written as

$$\dot{\rho} = -\frac{i}{\hbar}[H_0, \rho] + \sum_{ij} \Gamma_{ij} (\sigma_{ji} \rho \sigma_{ij} - \frac{1}{2} \{\sigma_{ij} \sigma_{ji}, \rho\}), \quad (11)$$

where $\Gamma_{ij} = \Gamma_{ijji}(\infty)$.

C. Environment: Spectral densities

Obviously, the spectral densities defining the transition rates are related to those in the original basis. In particular,

$$\begin{aligned} \tilde{R}_{-++-}(\omega) &= \frac{1}{4} \sin^2 \theta [R_{2222}(\omega) \\ &\quad - R_{22BB}(\omega) - R_{BB22}(\omega) + R_{BBBB}(\omega)], \\ \tilde{R}_{A\pm\pm A}(\omega) &= \frac{1}{2} (1 \pm \cos \theta) R_{ABBA}, \end{aligned} \quad (12)$$

with $\mathcal{R}_{jiji}(\omega) = \mathcal{R}_{ijji}(\omega)$.

It is clear that the relevant spectral densities \tilde{R}_{ijji} describing the transitions between Coulomb-correlated X-BX configurations are combinations of the spectral densities $R_{\alpha\beta\gamma\delta}$ that describe dephasing and interband relaxation between X and BX states. Interestingly, the transition between the two Coulomb-mixed states, that is, the impact ionization process, described by $\tilde{R}_{\mp\pm\mp\mp}$ is entirely related to the diagonal couplings between the original states and the environment. Obviously, the corresponding rate vanishes for small X-BX mixing as $\theta^2 \sim [V/(\epsilon_B - \epsilon_2)]^2$. On the other hand, the transition to the other X state A (relaxation or impact ionization) is governed by the off-diagonal couplings, which are related to intraband relaxation between these states. If the diagonal and off-diagonal couplings are of similar magnitude (as it is the case, e.g., for carrier-phonon couplings), then the impact ionization and Auger recombination are formally suppressed by a factor $\sin^2 \theta$ or $\sin^2 \theta/2$ as compared to relaxation. However, as we will show below, what really matters is the frequency dependence of the reservoir spectral density which can make the impact ionization process favorable, depending on the X-BX level alignment.

The details of the system-environment coupling may vary for different nanocrystal systems and, to our knowledge no general microscopic theory has been proposed for its exact treatment. Hence, in most of our simulation, we take the spectral densities in the original basis in the simplest Ohmic form, $R_{\alpha\beta\gamma\delta}(\omega) = a_{\alpha\beta\gamma\delta} [n_B(\omega) + 1] J(\omega)$, where $J(\omega) = (J_0 \omega / \omega_0) \exp[-(\omega / \omega_0)^2]$ (see Sec. III B for comparison with a super-ohmic case).

Here, $n_B(\omega)$ is the Boltzmann distribution function, J_0 is the overall magnitude of the dissipation and ω_0 is the cut-off frequency. In the simplest case of lowest-order acoustic phonon processes, ω_0 is on the order of R/c , where c is the speed of sound, which yields a

value on the order of ps^{-1} . This can be different if multiple-phonon processes are included. The values of the coefficients $a_{\alpha\beta\gamma\delta}$ follow from the physical nature of the carrier-environment coupling: The spectral densities $R_{\alpha\alpha\beta\beta}(\omega)$ result from diagonal couplings between the carriers in the NC and their environment. It seems reasonable to assume that these couplings are at least approximately proportional to the charge density (this is true, e.g., for carrier-phonon couplings as well as for Coulomb couplings to fluctuating background or impurity charge). Thus, typically, $\mathcal{R}_{22} = 2\mathcal{R}_{BB}$ and, in consequence, $a_{22BB} = a_{BB22} = 2$, $a_{2222} = 4$ and $a_{\alpha\beta\gamma\delta} = 1$ otherwise.

As we will show, the system dynamics in the dissipative MEG process depends to some extent on the excitation conditions. Nevertheless, instead of including the electromagnetic field explicitly in our simulation we note that the excitation may fall essentially in three classes: a short (spectrally broad) pulse excites an optically active (bright) X state, a long (spectrally narrow) pulse excites selectively an eigenstate of the system and broad band thermal radiation excites an incoherent mixture of system eigenstates, proportionally to their overlap with the bright X state (see Appendix for details). Thus, as the initial state we take the state $|B\rangle$, corresponding to an ultra fast coherent excitation (a broad band laser pulse), a pure $|+\rangle$ or $|-\rangle$ state for a narrow band laser pulse or a mixture of the eigenstates $|+\rangle$ and $|-\rangle$, corresponding to incoherent excitation by thermal radiation.

III. RESULTS

A. Dissipative MEG dynamics

Several parameters play a crucial role in the dissipative MEG process: the energy differences between the X state A, the excited state B and the BX state 2, the Coulomb coupling between the X and BX states, and the parameters governing the dissipative relaxation process (the magnitude J_0 and the frequency cut-off ω_0). In this section, we study the dynamics of the dissipative MEG process for various energetical alignment of the states, assuming fixed values of the dissipation parameters, and compared the results to the case without dissipation.

In the absence of Coulomb coupling, there is no mechanism for a transition to the BX state (this state is completely decoupled), hence, only relaxation between the states B and A takes place. This is shown in Fig. 3 (the dynamics in this case is independent of the excitation conditions). In this case, the BX state is indeed never occupied and the total number of excitons, N_x , remains equal to one. The only occurring process is the intraband occupation transfer from the initial state B to the dark X state A.

The variation of the state occupations and the average number of excitons in the presence of a realistic Coulomb coupling ($V_B = 1$ meV) is shown in Fig. 4 for the case

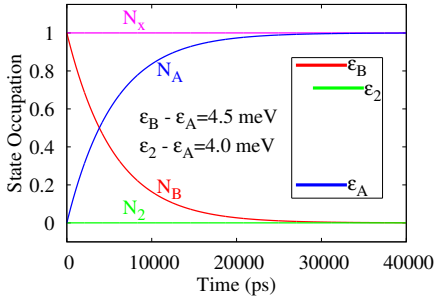


FIG. 3. (Color online) The variation of the state occupations N_A , N_B and N_2 and the average number of excitons N_x in the absence of Coulomb coupling at $T = 0$ K.

of coherent ultrafast excitation. As mentioned above, under these excitation conditions, the initial system state is $|B\rangle$, hence $N_x = 1$. When the bright state $|B\rangle$ and the BX state $|2\rangle$ are close to each other, Fig. 4(a,b), the Coulomb interaction leads to strong mixing of the states $|B\rangle$ and $|2\rangle$. As a result, transition between the resulting eigenstates are efficient which means that the dissipative impact ionization is very fast as manifested by the rapid growth (below 1 ps) of the occupation of the state $|2\rangle$ and the corresponding increase of the average number of excitons (the lower eigenstate is still predominantly bi-excitonic). Since the initial state $|B\rangle$ is a superposition of system eigenstates, there is an intense oscillation at the beginning of the process but its amplitude goes to zero in about 10 ps. Later on the system relaxes to the state $|A\rangle$, which corresponds to the Auger recombination. The BX state decays in this process on a time scale of about 150 ps. The slow rate of the Auger process is due to the relatively large energy distance to the state A , which makes the relaxation to this state ineffective.

For another configuration, Fig. 4(c,d), when the BX state is shifted closer to the state $|A\rangle$, the relaxation behavior does not change significantly. However, the maximum occupation of the state $|2\rangle$ is much lower. This results from the larger energy spacing between the states which is beyond the frequency cut-off of the spectral density, which considerably suppresses the relaxation to the state $|-\rangle$ which is a predominantly BX state. Thus, in the competition between the impact ionization (transition to the state $|-\rangle$ or, almost equivalently, to the BX state $|2\rangle$) and the usual relaxation (transition to $|A\rangle$), the latter starts to dominate. In addition, the similar energy spacings $\epsilon_B - \epsilon_2$ and $\epsilon_2 - \epsilon_A$ makes the Auger recombination from the state $|2\rangle$ to the state A much more effective in comparison to the impact ionization. In this case, the oscillation amplitude decays in a slightly longer time of a few tens of picoseconds. In both of these configurations, the impact ionization competes strongly also with the Auger recombination, the latter being faster in the second configuration.

In the absence of dissipation, $J_0 = 0$, for both the above mentioned configurations, the average number of

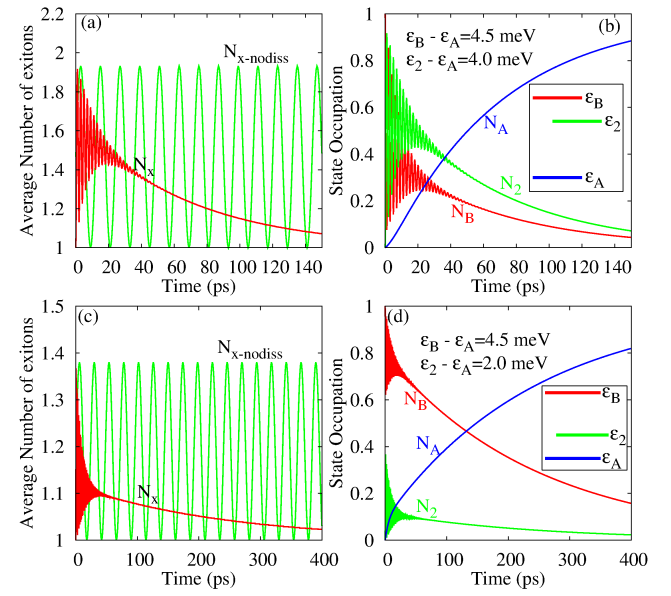


FIG. 4. (Color online) The occupations of the system states (right panels) and the average number of excitons (left panels) for $V_B = 1$ meV for 2 possible alignments of the energy levels at $T = 0$ K. In the left panels, the average number of excitons in the case without dissipation. Coherent ultrafast excitation is assumed here.

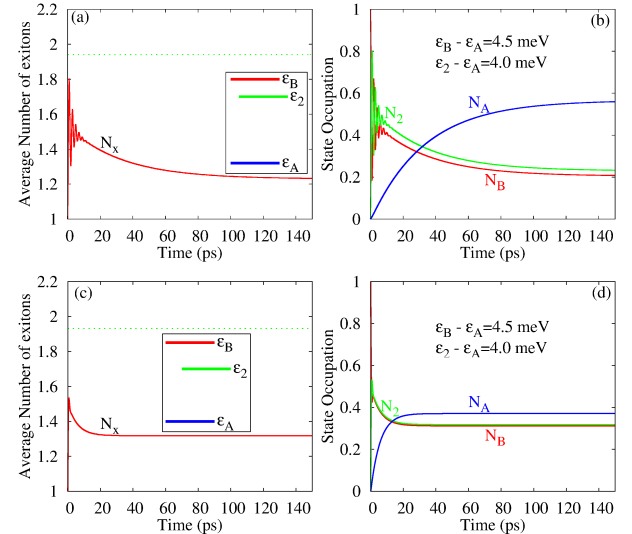


FIG. 5. (Color online) As in Fig. 4 but at $T = 50$ K (a,b) and $T = 300$ K (c,d).

excitons oscillates constantly (green lines in Fig. 4(a,c)). However, as one could expect, the amplitude of the oscillation is different for various configurations due to different degrees of mixing between the eigenstates. Note that for the first alignment (Fig. 4(a,b)), the number of excitons generated in the presence of dissipation is larger than that achieved without dissipation (taking the average of oscillation in both cases).

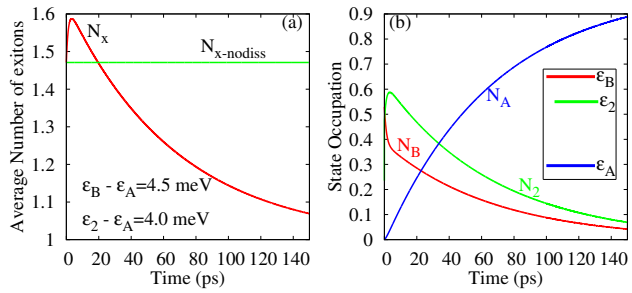


FIG. 6. (Color online) The dynamics of (a) the average number of excitons (b) the system state occupations for incoherent excitation by thermal radiation at $T = 0$ K. In (a), the average number of excitons in the case without dissipation is also shown (green line).

At higher temperature, $T = 50$ K, Fig. 5(a,b), the relaxation dynamics does not change considerably but, the oscillation amplitude decays in a shorter time. At $T = 300$ K, Fig. 5(c,d), the initial average number of excitons is slightly decreased and the oscillations vanish quickly. The final average number of excitons goes up at higher temperatures because of nonzero thermal occupations.

Under incoherent excitation, according to the Fermi golden rule, the system eigenstates are excited proportionally to their coupling to the light, that is, to the admixture of the bright state $|B\rangle$. Since in the presence of the Coulomb coupling, the eigenstates $|+\rangle$ and $|-\rangle$ are superpositions of the original X state $|B\rangle$ and BX state $|2\rangle$, they are characterized by the average number of exciton between 1 and 2. Hence, the initial number of excitons may exceed 1. The system dynamics in this case, shown in Fig. 6 for one of the level alignments, is very similar to that following a coherent excitation but no oscillations are seen since no coherence between the eigenstates is present. There is again a strong competition between the impact ionization, the X relaxation and the Auger recombination. As a result, the occupation of the BX state again grows rapidly and then decays completely on a longer time scale.

Under these excitation conditions, in the absence of dissipation, the average number of excitons would remain constant but in the presence of dissipation it increases considerably to a maximum value and then decays. It is clear that the maximum average number of excitons resulting from the dissipative MEG dynamics in this case exceeds that following the excitation in the absence of dissipation. This is due to the dissipative transition to the predominantly biexcitonic state $|-\rangle$, which develop on a time scale much shorter than the subsequent Auger transition to the lowest state $|A\rangle$.

It can be seen by comparing Fig. 6 and Fig. 4 that for incoherent excitation, the value of the average number of excitons is equal to the mean value of the oscillations that could be seen in Fig. 4. The same holds true also for the other level alignments, not shown in Fig. 6.

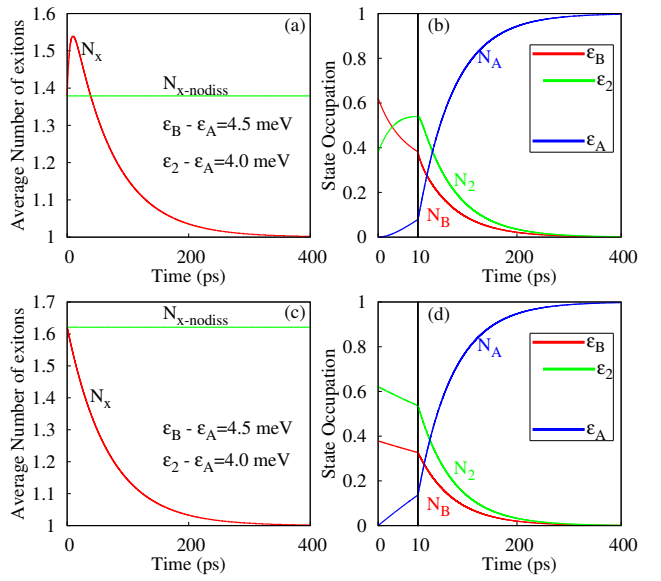


FIG. 7. (Color online) The variation of state occupation and the average number of excitons as a function of time at $T = 0$ K. (a,b) for the initial state $|+\rangle$; (c,d) for the initial state $|-\rangle$ (narrow band excitation). In (b,d), the initial 10ps of the evolution is expanded.

Under the third possible excitation conditions, when a spectrally narrow light field is used, a light beam is tuned to excite just the state $|-\rangle$ or $|+\rangle$ (see Appendix for details). These two cases are compared in Fig. 7. One can see that the only difference between starting from $|+\rangle$ or $|-\rangle$ is the behavior of the BX occupation at the very beginning of the evolution, which rises during the first few ps for the initial state $|+\rangle$ (Fig. 7(b)), which can easily be explained. Since the energy of the state $|+\rangle$ is higher than the energy of the state $|-\rangle$, starting with the state $|+\rangle$ will cause the transition from $|+\rangle$ to $|-\rangle$. After this initial redistribution of occupation, the occupations of the states do not depend on the initial conditions. This is in contrast with the case without dissipation where the average number of excitons remains about 1.4 and 1.6 in the case of starting from $|+\rangle$ and $|-\rangle$, respectively, in accordance with the composition of these eigenstates in terms of the X and BX states. Obviously, no oscillations can be observed in the evolution of the system which was initially prepared in one of the eigenstates $|+\rangle$ or $|-\rangle$.

In order to understand the dependence of the observed dynamics on the energy spacing between the levels, we will now discuss the case when the energy differences between the states are 1.4 times larger than the set of parameters in Fig. 4. The dissipation parameters $J_0 = 1 \text{ ps}^{-1}$ and $\omega_0 = 2 \text{ ps}^{-1}$ are kept unchanged. The results of the simulations are shown in Fig. 8. The impact ionization now appears in a shorter time interval (about 10 ps). If the state $|2\rangle$ lies close to the state $|B\rangle$ [Fig. 8(a,b)], because of the large energy difference between the states $|+\rangle$, $|-\rangle$ and $|A\rangle$ (beyond the cut-off

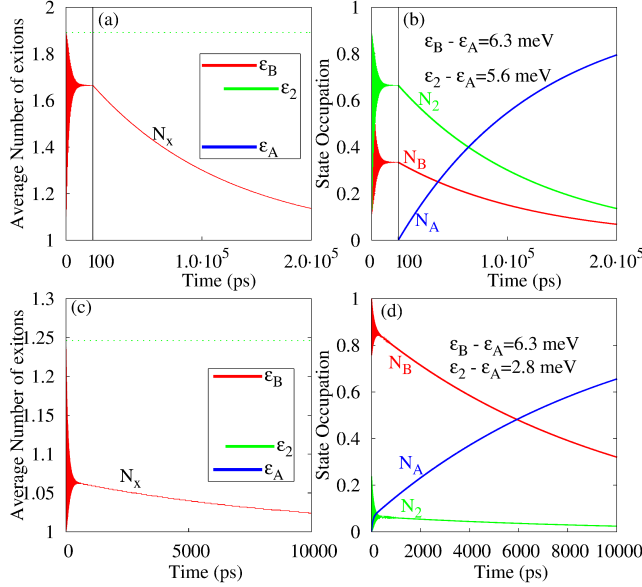


FIG. 8. (Color online) The state occupations (right panels) and the average number of excitons (left panels) for 2 alignments of the energy levels in the case of increased energy difference between the states (1.4 times larger than Fig. 4) at $T = 0$ K. In the left panels, the upper envelope of the oscillations of the average number of excitons in the case without dissipation is also shown (green dotted line). Coherent ultrafast excitation is assumed here.

energy $\hbar\omega_0$), the rate of the Auger recombination is decreased as compared to the previous case and the BX occupation persists much longer. The oscillation amplitude is much lower than in the previous case (due to a smaller mixing between the X and BX states) and decays rapidly (in a few ps). As it is depicted in Fig. 8(c,d), when the BX state gets closer to the state A, the degree of the impact ionization decreases dramatically. Besides, oscillation amplitude decays in a much longer time of a few hundreds of picoseconds. The achieved number of excitons is much lower than in all the previously discussed cases.

At higher temperature, Fig. 9, the impact ionization process takes place on the time scale of several picoseconds (decreasing with increasing temperature) and is then followed by a slow Auger recombination on the order of nanoseconds for this set of parameters).

In a realistic sample, one deals with an ensemble of nanocrystals with a certain size dispersion. To obtain the dynamics for the whole nanocrystal ensemble, we average our results over the energy of the BX state $|2\rangle$ which can be different for each single nanocrystal. We use a Gaussian distribution for the value of ϵ_2 ,

$$f(\epsilon_2) = \frac{1}{\sqrt{2\pi}\sigma} e^{-\frac{1}{2}(\frac{\Delta E}{\sigma})^2}, \quad (13)$$

where $\Delta E = \epsilon_2 - \epsilon_{20}$ and σ is a standard deviation, while

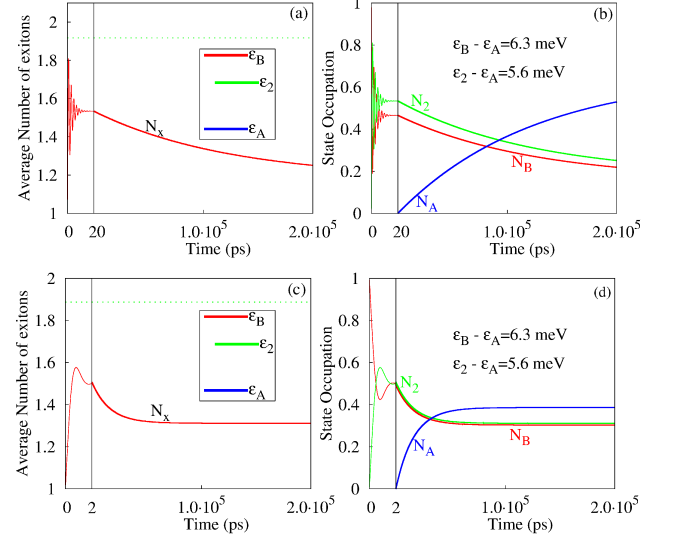


FIG. 9. (Color online) As in Fig. 8 but for $T = 50$ K (a,b) and $T = 300$ K (c,d).

keeping ϵ_A and ϵ_B constant.

The results are shown in Fig. 10 for different sets of parameters. In Figs. 10(a,c,e), we fix the mean BX energy ϵ_{20} at 4 meV and the energy ϵ_B at 4.5 meV above ϵ_A and show the results for three different values of σ . In Figs. 10(b,d,f), a small standard deviation, $\sigma = 1$ meV is chosen and the results for two different level alignments are shown.

Comparison of Fig. 10 with Figs. 4 and 5 shows that a small inhomogeneity of the level alignment in the ensemble (red lines in Figs. 10(a,c,e)) does not change the overall system dynamics. The amplitude of the oscillations at $T = 0$ is reduced due to ensemble dephasing but the average trend is almost exactly the same. This is true for all the level alignments studied here, and at all temperatures, as can be seen in Figs. 10(b,d,f). On the other hand, increasing the inhomogeneity reduces the amplitude of the initial peak of the average number of excitons, in particular at higher temperatures, and leads to a nearly featureless time dependence of this quantity after the initial ultrafast growth. For larger inhomogeneities, also the overall (long time) value of the average number of excitons is reduced. This suppression of the MEG efficiency in the ensemble in our model is due to the fact that in a strongly inhomogeneous ensemble the contribution from NCs with very distant levels becomes larger.

B. Non-Markovian corrections

In this section, we discuss some further technical aspects of the modeling of the MEG dynamics in NCs. We assess the corrections due to the reservoir memory (beyond the Markov approximation) and study the differences between Ohmic and super-Ohmic reservoir models.

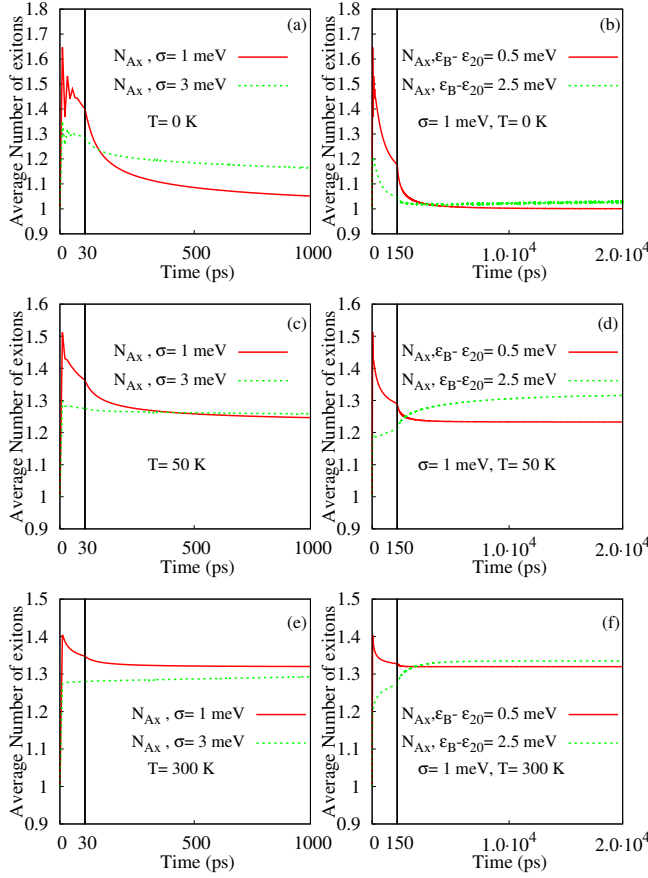


FIG. 10. (Color online) The variation of the average number of excitons as a function of time at three different temperatures. Left panels: for two different values of σ . Right panels: for two different energies of the BX state for $\sigma = 1$ meV. (a,b) $T = 0$ K, (c,d) $T = 50$ K and (e,f) $T = 300$ K. Ultra fast excitation conditions is assumed here.

In Fig. 11, we compare the simulation results for one selected set of system parameters obtained from the Lindblad equation (red solid lines) and from the non-Markovian TCL equation (blue dashed lines). In order to understand the role of various approximations made on the way to the Markovian description in terms of the Lindblad equation, we present also results following from two kinds of secular approximations to the TCL equation (green dotted and gray dash-dotted lines). In the approximation labeled “SEC.1”, only the rates $\Gamma_{ijji}(t)$ appearing in the Lindblad equation are kept (but no Markovian approximation is made, which is reflected on the level of the TCL equation by the time dependence of the rates). In the second secular approximation, denoted “SEC.2”, also the other subset of secular rates, $\Gamma_{iiji}(t)$ is retained. At long times, these rates become proportional to the spectral density at zero frequency, hence they tend to zero in the zero temperature limit. Therefore, at low temperatures, they are only important in the initial period of the dynamics (for times on the order of $1/\omega_0$),

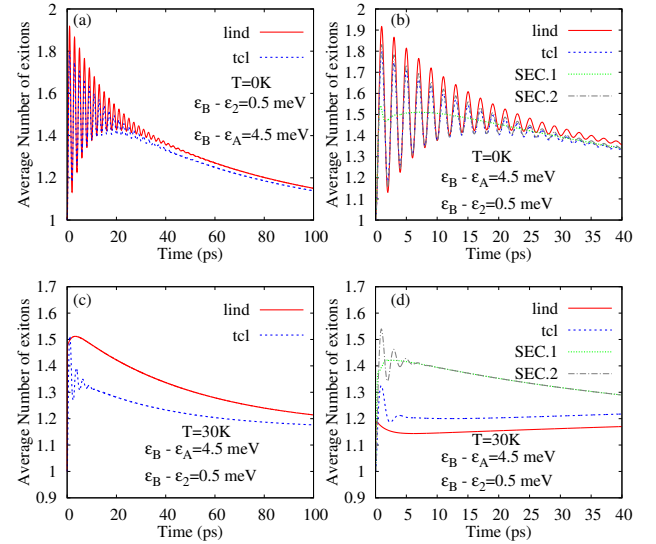


FIG. 11. Comparison of the simulation results using different Markovian and non-Markovian approximations.

when non-Markovian effects are dominant.

As one can see in Fig. 11(a), at zero temperature the corrections to the Markovian dynamics are rather small and essentially amount to a reduced amplitude of the oscillations observed during the first few tens of picoseconds after the excitation. Both the time-averaged value of this oscillating exciton number as well as the long-time asymptotics are nearly the same in both cases. This is also visible in Fig. 11(b), where the initial period of time is shown in more detail. A close look at the curves reveals that the difference between the Lindblad and TCL results is due to initial damping within a few picoseconds from the initial time, while the subsequent evolution is characterized by the same exponential damping of the oscillations and decay of the populations in both cases. This initial damping is due to the fact that the short-time values of the non-Markovian damping rates involve interaction with the whole reservoir spectrum, while in the Markov limit only the resonant modes are involved, corresponding to the relatively low values of the spectral density in its high-energy tails in the present case.

In Fig. 11(b), we have also displayed the results obtained from the non-Markovian TCL equations in which the non-secular (oscillating) terms have been removed. It is clear that both classes of secular terms must be kept in the non-Markovian description even though only one of them appears in the Lindblad equation which yields quite accurate results. Otherwise, the initial, non-Markovian damping is overestimated by an order of magnitude. Still, however, the trend is reproduced correctly. Similar effect, although with a larger quantitative difference in the oscillation amplitudes, is seen in a system with lower energy spacing between the levels (not shown here).

A similar comparison for $T = 30$ K, presented in Fig. 11(c), shows a larger difference between the Marko-

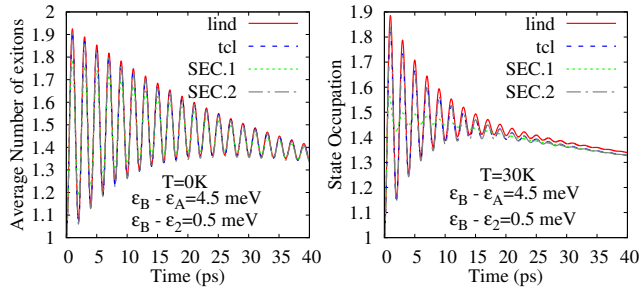


FIG. 12. Comparison of the Markovian and non-Markovian approximations for an Ohmic and super-Ohmic reservoir.

vian and non-Markovian modeling results. Now, the Markov approximation overestimates the damping of the initial oscillations and yields a higher number of excitons (the latter depends on the level alignment; we have observed an opposite situation for smaller inter-level spacings, not shown here). Much more interesting is the analysis of the role of secular vs. Markov approximations in this moderate temperature case, shown in Fig. 11(d). Here, both secular approximations yield the same long-time asymptotics but differ in the way the initial oscillations are reproduced: if only the terms entering in the Lindblad equation are kept the oscillations vanish completely, as is also the case for the Lindblad description. The other, more complete secular approximation, reproduces the oscillations qualitatively correctly, although with a shift of the average trend. Even in this case, however, the quantitative characteristics of the MEG process are very similar in all the approximations.

So far, in all our simulations we have assumed a reservoir with Ohmic spectral characteristics ($J(\omega) \sim \omega$ at $\omega \rightarrow 0$). This is the standard choice for generic modeling of the dynamics of an open quantum system in the absence of any detailed knowledge about the particular reservoir in question and has also been employed in some studies of the dissipative MEG process³⁶. However, some specific reservoirs are known to have other spectral characteristics. In particular, the three-dimensional acoustic phonon reservoir shows a super-Ohmic behavior with $J(\omega) \sim \omega^3$ at $\omega \rightarrow 0$. This leads to vanishing spectral densities $R(\omega)$ at $\omega = 0$ and, as mentioned above, to suppression of a class of damping rates in the long time limit. It seems interesting to study how this qualitative difference affects the system dynamics both in the Markov limit and in the non-Markovian model. To this end, in Fig. 12, we show the simulation results for the same system as in Fig. 11 but with a super-Ohmic spectral density $J(\omega) = J_0(\omega/\omega_0)^3 \exp(-\omega^2/\omega_0^2)$ with the amplitude J_0 and cut-off frequency ω_0 chosen in such a way that the Markovian transition rates from the states $|+\rangle$ and $|-\rangle$ to the state $|A\rangle$ are the same as in the previous Ohmic case. The zero temperature results presented in Fig. 12(a) show a very similar behavior to the Ohmic case at the same temperature [Fig. 11(b)] but much less

sensitivity to the approximation used. In particular comparison between the results obtained with various secular approximations shows that the dynamics is determined by the Lindblad rates Γ_{ijji} . This can be attributed to the reduced magnitude of the spectral density in the vicinity of $\omega = 0$, which reduces the role of the other secular rates not only in the long time limit but also already for shorter times. This role of the secular terms of the second type is larger at higher temperatures [Fig. 12(b)], where neglecting them leads to strongly overestimated damping. Remarkably, the non-Markovian corrections are much smaller in the super-Ohmic case and both the average trend of the evolution of the exciton number as well as the long-time value are nearly the same here, in contrast to the Ohmic model (especially at higher temperatures).

IV. CONCLUSIONS

We have formulated and studied a few-level model of dissipative multiple exciton generation and relaxation dynamics following a photon absorption in a semiconductor nanocrystal. We have accounted for the interaction with the reservoir by introducing a physically motivated set of spectral densities which allowed us to relate the impact ionization and Auger relaxation rates to the diagonal and off-diagonal carrier-reservoir couplings, respectively, and to highlight the role of the interband Coulomb coupling for the magnitudes of the rates governing these two processes.

With this model, we have solved the Markovian quantum Master (Lindblad) equation to investigate the impact of dissipation on the evolution of the single- and bi-exciton occupation. We have shown that the system evolution strongly changes if the dissipation is included. In many cases, the maximum average number of electron-hole pairs (i.e., the efficiency of the MEG process) is increased if dissipative transitions are allowed and can be close to 2. Thus, dissipation can play a constructive role in the MEG process and is not necessarily a competing factor^{26,30,31}. In a certain range of parameters, the growth of the exciton number (MEG process) is very fast (on picosecond time scale) and the following decay of the biexciton population (Auger process) is much slower (on the time scale of hundreds of picoseconds), which means that such a dissipative dynamics following an ultrafast excitation cannot be excluded based on the observed very fast time scale of the process³. In addition, the differences between the system dynamics under various excitation conditions, which are present in the dynamics of an isolated nanocrystal, are washed out by fast reservoir-induced dephasing. We have verified also that similar dissipation-related features in the system kinetics are observed in an inhomogeneous ensemble of nanocrystals.

We have studied also the sensitivity of the modeling results to various formal characteristics of the model. We

have shown that the dynamics very strongly depends on the position of the high-frequency cut-off of the reservoir spectral density. The simulated dynamics depends to some extent on the chosen class of the reservoir models but the observed differences between the Ohmic and super-Ohmic models are mostly of quantitative character and change neither the qualitative features of the dynamics nor the quantitative expectations for an overall MEG yield in a nanocrystal ensemble. We have investigated also the role of non-Markovian corrections to the system dynamics. Although the evolution found from non-Markovian equations differs in some cases from that obtained in the Markov limit these discrepancies mostly have the form of oscillations that are present only during the first few tens of picoseconds after excitation and are not expected to affect the overall quantitative predictions for the MEG yield.

V. ACKNOWLEDGMENTS

This work was supported by the TEAM programme of the Foundation for Polish Science co-financed from the European Regional Development Fund.

VI. APPENDIX: THE DENSITY MATRIX ELEMENTS CORRESPONDING TO VARIOUS EXCITATION CONDITIONS

In this appendix, we derive the state occupations after optical excitation in various excitation conditions. First, we consider the interaction between a strong coherent field (as a pulsed excitation treated classically) and our 4 levels system. A single mode radiation source, such a laser, will produce an electromagnetic wave with amplitude $\mathcal{E}_0(t)$ and frequency Ω ,

$$\mathcal{E}(t) = \mathcal{E}_0(t) \cos \Omega t. \quad (14)$$

The interaction Hamiltonian between this electromagnetic wave and our system is

$$H_{\text{int}} = -\mathbf{d} \cdot \mathcal{E}(t) = f(t) \cos \Omega t (|G\rangle\langle B| + \text{h.c.}), \quad (15)$$

where we defined $f(t) = -\mathbf{d} \cdot \mathcal{E}_0(t)$. In the eigenbasis $(|+\rangle, |-\rangle)$ and in the rotating wave approximation, we have

$$H_{\text{int}} = \frac{1}{2} f(t) (|G\rangle\langle +| e^{i\Delta_{\pm} t} \cos \frac{\theta}{2} - |G\rangle\langle -| e^{i\Delta_{\pm} t} \sin \frac{\theta}{2} + \text{h.c.}), \quad (16)$$

where $\Delta_{\pm} = \Omega - \frac{E_{\pm}}{\hbar}$ is the detuning from the transition energy. The system state after the optical pulse up to the 2nd order in $\mathcal{E}_0(t)$ is

$$\rho = \rho_0 - \frac{i}{\hbar} \int_{-\infty}^{\infty} dt [H_{\text{int}}, \rho_0] - \frac{1}{2\hbar^2} \int_{-\infty}^{\infty} dt \int_{-\infty}^t d\tau [H_{\text{int}} [H_{\text{int}}, \rho_0]], \quad (17)$$

where $\rho_0 = |G\rangle\langle G|$. The occupations of the $|+\rangle$ and $|-\rangle$ states appear in the 2nd order term, assuming a Gaussian envelope for $f(t)$,

$$f(t) = \frac{1}{\sqrt{2\pi\tau}} e^{-\frac{1}{2}(\frac{t}{\tau})^2}, \quad (18)$$

one finds the density matrix elements corresponding to the coherent excitation in the form

$$\begin{aligned} \langle \pm | \rho | \pm \rangle &= \frac{1}{\sqrt{2\pi\tau}} \frac{1 \pm \cos \theta}{2} e^{-\tau^2 \Delta_{\pm}^2} \\ \langle + | \rho | - \rangle &= \langle - | \rho | + \rangle = -\frac{1}{2\sqrt{2\pi\tau}} \sin \theta e^{-\frac{\tau^2}{2} (\Delta_{+}^2 + \Delta_{-}^2)} \end{aligned} \quad (19)$$

where τ is the pulse duration.

In the case of a narrow band excitation condition, when $\Delta_{\pm}\tau \gg 1$, all the exponents in Eq. (19) vanish except for the one corresponding to $\Delta_{\pm} = 0$. Thus the only non-zero element will be $\langle - | \rho | - \rangle$ or $\langle + | \rho | + \rangle$ corresponding to the laser tuned to Δ_- or Δ_+ , respectively. On the other hand, for a broad band excitation condition (short pulse), $\Delta_{\pm}\tau \ll 1$, all the exponents in Eq. (19) are almost equal to 1. After inverting Eq. (4) and substituting to Eq. (19) one finds $\langle B | \rho | B \rangle = 1$ and $\langle 2 | \rho | 2 \rangle = 0$. Hence, under this conditions, only the state $|B\rangle$ is excited.

Second, let us consider broad band thermal radiation. Then an incoherent mixture of system eigenstates is excited, so that there is no coherence between the $|+\rangle$ and $|-\rangle$ states. The interaction Hamiltonian is described by

$$\begin{aligned} H_{\text{int}} &= \mathbf{d} \cdot \mathcal{E} = \sum_{k\lambda} g_{k\lambda} (b_{k\lambda} + b_{k\lambda}^{\dagger}) \\ &\times (|G\rangle\langle A| + \cos \left(\frac{\theta}{2} \right) |G\rangle\langle +| - \sin \left(\frac{\theta}{2} \right) |G\rangle\langle -| + \text{h.c.}), \end{aligned} \quad (20)$$

where $b_{k\lambda}$ and $b_{k\lambda}^{\dagger}$ are photon annihilation and creation operators respectively. The occupation of the system states resulting from this kind of excitation are proportional to the corresponding transition states, which can be found using the Fermi golden rule. Since the states $|+\rangle$ and $|-\rangle$ are very close compared to the photon energy, the difference in the photon density of states and coupling magnitude is negligible and one finds up to a constant.

$$\begin{aligned} \langle \pm | \rho | \pm \rangle &\sim \frac{1 \pm \cos \theta}{2}, \\ \langle + | \rho | - \rangle &= \langle - | \rho | + \rangle = 0. \end{aligned} \quad (21)$$

¹ A. J. Nozik, *Physica E* **14**, 115 (2002).

² R. D. Schaller and V. I. Klimov, *Phys. Rev. Lett.* **92**, 186601 (2004).

³ R. D. Schaller, V. M. Agranovich, and V. I. Klimov, *Nat. Phys.* **1**, 189 (2005).

⁴ R. Ellingson, M. Beard, J. Johnson, P. Yu, O. Micic, A. Nozik, A. Shabaev, and A. Efros, *Nano Lett.* **5**, 865 (2005).

⁵ R. D. Schaller, M. Sykora, J. M. Pietryga, and V. I. Klimov, *Nano Lett.* **6**, 424 (2006).

⁶ R. Schaller, J. Pietryga, and V. Klimov, *Nano Letters* **7**, 3469 (2007).

⁷ J. J. H. Pijpers, E. Hendry, M. T. W. Milder, R. Fanciulli, J. Savolainen, J. L. Herek, D. Vanmaekelbergh, S. Ruhman, D. Mocatta, D. Oron, A. Aharoni, U. Banin, and M. Bonn, *J. Phys. Chem. C* **111**, 4146 (2007).

⁸ M. C. Beard, K. P. Knutson, P. Yu, J. M. Luther, Q. Song, W. K. Metzger, R. J. Ellingson, and A. J. Nozik, *Nano Lett.* **7**, 2506 (2007).

⁹ M. Ji, S. Park, S. T. Connor, T. Mokari, Y. Cui, and K. J. Gaffney, *Nano Lett.* **9**, 1217 (2009).

¹⁰ G. Nair and M. G. Bawendi, *Phys. Rev. B* **76**, 081304 (2007).

¹¹ M. T. Trinh, A. J. Houtepen, J. M. Schins, T. Hanrath, J. Piris, W. Knulst, A. P. L. M. Goossens, and L. D. A. Siebbeles, *Nano Lett.* **8**, 1713 (2008).

¹² J. J. H. Pijpers, E. Hendry, M. T. W. Milder, R. Fanciulli, J. Savolainen, J. L. Herek, D. Vanmaekelbergh, S. Ruhman, D. Mocatta, D. Oron, A. Aharoni, U. Banin, and M. Bonn, *J. Phys. Chem. C* **112**, 4783 (2008).

¹³ M. Ben-Lulu, D. Mocatta, M. Bonn, U. Banin, and S. Ruhman, *Nano Lett.* **8**, 1207 (2008).

¹⁴ G. Nair, S. M. Geyer, L.-Y. Chang, and M. G. Bawendi, *Phys. Rev. B* **78**, 125325 (2008).

¹⁵ J. A. McGuire, J. Joo, J. M. Pietryga, R. D. Schaller, and V. I. Klimov, *Accounts Chem. Res.* **41**, 1810 (2008).

¹⁶ J. A. McGuire, M. Sykora, J. Joo, J. M. Pietryga, and V. I. Klimov, *Nano Lett.* **10**, 2049 (2010).

¹⁷ D. J. Binks, *Phys. Chem. Chem. Phys.* **13**, 12693 (2011).

¹⁸ J. B. Sambur, T. Novet, and B. A. Parkinson, *Science* **330**, 63 (2010).

¹⁹ O. E. Semonin, J. M. Luther, S. Choi, H.-Y. Chen, J. Gao, A. J. Nozik, and M. C. Beard, *Science* **334**, 1530 (2011).

²⁰ K. Hyeon-Deuk and O. V. Prezhdo, *Nano Lett.* **11**, 1845 (2011).

²¹ K. Hyeon-Deuk and O. V. Prezhdo, *ACS Nano* **6**, 1239 (2012).

²² A. Franceschetti, J. M. An, and A. Zunger, *Nano Lett.* **6**, 2191 (2006).

²³ E. Rabani and R. Baer, *Nano Lett.* **8**, 4488 (2008).

²⁴ M. Califano, *ACS Nano* **3**, 2706 (2009).

²⁵ R. Baer and E. Rabani, *Nano Lett.* **12**, 2123 (2012).

²⁶ G. Allan and C. Delerue, *Phys. Rev. B* **73**, 205423 (2006).

²⁷ C. Delerue, G. Allan, J. J. H. Pijpers, and M. Bonn, *Phys. Rev. B* **81**, 125306 (2010).

²⁸ M. Korkusinski, O. Voznyy, and P. Hawrylak, *Phys. Rev. B* **82**, 245304 (2010).

²⁹ M. Korkusinski, O. Voznyy, and P. Hawrylak, *Phys. Rev. B* **84**, 155327 (2011).

³⁰ A. Shabaev, A. L. Efros, and A. J. Nozik, *Nano Lett.* **6**, 2856 (2006).

³¹ W. M. Witzel, A. Shabaev, C. S. Hellberg, V. L. Jacobs, and A. L. Efros, *Phys. Rev. Lett.* **105**, 137401 (2010).

³² L. Silvestri and V. M. Agranovich, *Phys. Rev. B* **81**, 205302 (2010).

³³ F. Schulze, M. Schloth, U. Woggon, A. Knorr, and C. Weber, *Phys. Rev. B* **84**, 125318 (2011).

³⁴ E. Rabani and R. Baer, *Chem. Phys. Lett.* **496**, 227 (2010).

³⁵ A. Piryatinski and K. A. Velizhanin, *J. Chem. Phys.* **133**, 084508 (2010).

³⁶ K. A. Velizhanin and A. Piryatinski, *Phys. Rev. Lett.* **106**, 207401 (2011).

³⁷ P. Kowalski, L. Marcinowski, and P. Machnikowski, (arXiv:1208.2739).

³⁸ L. E. Brus, *J. Chem. Phys.* **80**, 4403 (1984).

³⁹ H.-P. Breuer and F. Petruccione, *The Theory of Open Quantum Systems* (Oxford University Press, Oxford, 2002).